We are IntechOpen, the world's leading publisher of Open Access books Built by scientists, for scientists

5,000
Open access books available

125,000
International authors and editors

140M
Downloads

Our authors are among the

154
Countries delivered to

TOP 1%
most cited scientists

12.2%
Contributors from top 500 universities

WEB OF SCIENCE™

Selection of our books indexed in the Book Citation Index in Web of Science™ Core Collection (BKCI)

Interested in publishing with us?
Contact book.department@intechopen.com

Numbers displayed above are based on latest data collected.
For more information visit www.intechopen.com

Chapter

Thermoelectric Properties of Chalcogenide System

Wiqar Hussain Shah and Waqas Muhammad Khan

Abstract

We will discuss the development of a new ternary and quaternary tellurium telluride chalcogenide nanoparticles used for efficient thermo-electric waste heat energy convertor called thermo-electric generator. Nanoparticles-based tellurium telluride chalcogenide nanoparticles, which will be used for thermoelectric generator, will eventually solve an important issue of the energy crises, that is, conversion of waste heat into useful electrical energy. By injecting charge carriers in the host matrix of $Tl_{10-x-y}A_xB_yTe_6$ nanomaterials system, different types of dopants (A = Pb, Sn, Ca and B = Pb, Sb Sr, etc.), with x = 0–2.5 and y = 0–2.5 on tellurium telluride has been introduced to synthesize new materials by Co-precipitation techniques and also by solid state reaction techniques followed by Ball-Milling for the fabrication of nanomaterials. We will study the effect of reduction of charge carriers in thermal and transport properties using different dopants contents by replacing host atoms. The charge carrier's concentration will affect the ratio of electron-hole concentration which in turns increases the electron scattering in these chalcogenide nanoparticles, which will affect the electrical conductivity and thermo-power. The prime purpose of doping with different ionic radii and different concentration is to enhance the power factor for the tellurium telluride nanosystem. At the end one will be able to control different physical parameters such as, thermally assisted electrical conductivity, and thermopower. Different characterization technique will be applied, for example, X-Ray diffraction techniques will be used for structural analysis, SEM will shows the morphological structure of the particles at 100 nm and energy dispersive x-rays spectroscopy will be used for elemental analysis. The electrical conductivity will be measured by four-probe resistivity measurement techniques, and Seebeck coefficient will be measured by standard temperature gradient techniques.

Keywords: effect of doping, Seebeck coefficient, electrical conductivity, power factor

1. Introduction

Energy storage and conversion devices (**Figure 1**) continue to be rich areas for scientific and engineering studies that incorporate novel features and functions in intelligent and interactive modes, represent a radical advance in consumer products, such as wearable electronics, healthcare devices, artificial intelligence, electric vehicles, smart household, and space satellites. However, there are still grand challenges in fundamental research and understanding to accelerate energy storage and

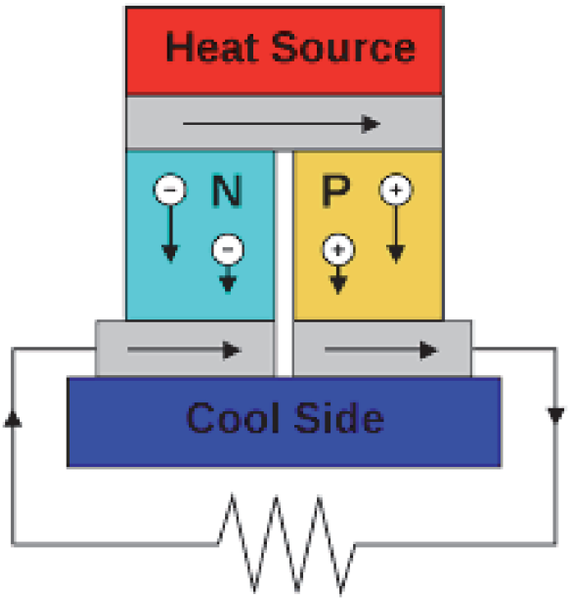

Figure 1.
Energy storage and conversion devices.

conversion devices to commercial reality, which include new materials and structures with high ionic conductivity, tailored mixed electron/ion conductivity, novel interface engineering methodologies, new device concepts, efficient and scalable techniques for materials and system-level integrations. This research study is intended to provide information for those working in energy storage and conversion devices from materials, characterizations, devices and system integrations to communicate recent progress on current technologies and to exchange ideas about next-generation solutions. In this research work, we will design and develop a new tellurium telluride chalcogenide materials used for efficient thermo-electric waste heat energy convertor called thermo-electric generator. Nanostructures based on tellurium telluride chalcogenide materials, which are used for efficient thermoelectric generator will eventually solve large issues of the energy crises.

Thomas john Seebeck discovered the effect of Seebeck on 14 December 1820, at famous science Academy of "Berlin" via detecting the deflection of magnetic compass needle nearby close ring of conducting wire that one adjacent is linked to metal of a low temperature while the second side is linked with metal of a high temperature. This effect recently verified that magnetic compass needle is bounced by reason of electrical current movement in wire and term "Thermo-magnetism" is changed by means of "the effect of thermoelectric". This electrical current/emf are similarly recognizing via means of "Seebeck emf." Thermo power "S" or Seebeck effect is the variation in electrical potential

$$(\Delta V = V_{hot} - V_{cold}) \tag{1}$$

Divided by the thermal gradient

$$(\Delta T = T\__{hot} - T\__{cold}), \tag{2}$$

Mathematically we can write it as,

$$S = \Delta V/\Delta T \tag{3}$$

$$S = (V\__{cold} - V\__{hot})/(T\__{hot} - T\__{cold})[V/K] \tag{4}$$

In 1834, The French watch maker and a part time physicist Jeane Chaarlese Athanaese Peltiere (1785–1845) published new research article in the French journal "Annal. Phy. Che," where Peltiere printed that by applying of electrical current in the direction of two dissimilar conductors, which are linked in series, disclosed that temperature changes by the side of joint of conductor. He recognized this specific effect as a "Peltier effect."

This particular effect can be mathematically written as,

$$Q = \Pi I \tag{5}$$

$$\Pi = \frac{Q}{I}\ [Watt/Ampere] \tag{6}$$

In upper formulation, the term "Q" representing degree by which warmth remains flow away per unit of time, while "Π" in formula is the "Peltiere coefficient" while the term "I" in upper formulation is electrical current which is formed in thermoelectric material (TEM).

Wiliam Thomoson in 1851 presented his well-known effect, which is named Thomson effect. "By means of creating a change in temperature "ΔT" crossways a conductor, wherein he displays association among Seebeck and Peltier effect."

Mathematically it can be written as,

$$\frac{dq}{dt} = -KJ\Delta T \tag{7}$$

In the above equation "K" is Thomson's coefficient and "J" is the density of current.

The Seebeck, The Peltiere and The Thomsen's coefficients are connected through the equation,

$$\Pi = TS \tag{8}$$

1.1 The Seebeck Coefficient

Once material is being heated through one side, then due to thermal gradient the thermoelectric voltage rises, since charge carriers (holes/electrons) drift from hot to ward cold. An induced voltage amount over a gradient of temperature

$$\left(S = \frac{\Delta V}{\Delta T}\right) \tag{9}$$

Among materials two (2) edges is recognized as per coefficient of Seebeck. Its unit is volt per kelvin (v/k).

When taking a Seebeck coefficient into its constituent, then written as below,

$$S = T\frac{8\pi^2 k_B^2 m^*}{3eh^2}\left(\frac{\pi}{3n}\right)^{2/3} \tag{10}$$

The above equation is Seebeck coefficient of degenerate semiconductors and metals. Above equation comprises of three (3) variables: Variable "T" signifies temperature, variable "n" signifies charge carrier concentration, besides variable "m^*" signifies "effective mass"

1.2 The electrical conductivity

Charge movement in matter is named conductivity, it is represented by "σ". The movement of holes or free electrons in a particular way reasons an electrical current in matter. This electrical current in matter which in a particular way, is the consequence of movement of charges via smearing the potential change crossways a semiconductor or conductor. The equation for current density "J" is;

$$J = nq\nu_d \tag{11}$$

In above equation, "n" signifies carrier concentration, the q in equation signifies charge carrier which is equivalents for holes to $+1.602 \times 10^{-19}C$ while $-1.602 \times 10^{-19}C$ for e's, and "ν_d" is called electron drift velocity. By means of putting value of drift velocity, $\nu_d = \frac{Ee\tau}{m^*}$ in Eq. (14), we obtained the relation which is used in the existence of constant electric field for current density, and this is as well-known as law of ohm.

$$J = \frac{ne^2\tau E}{m^*} \tag{12}$$

In terms of electrical conductivity and electric field, the current density J is,

$$J = \sigma E \tag{13}$$

$$\sigma = \frac{ne^2\tau}{m^*} = ne\mu \tag{14}$$

Where

$$\mu = \frac{e\tau}{m^*} \tag{15}$$

While "μ" is charge transporter movement and having dimension of $\left[\frac{cm^2}{Vs}\right]$. "$\tau$" is the scattering time while"m^*" is electron effective mass. The scattering time "τ" can be described as, "it is the amount of time in which the charge transporter their momentum is places besides turn out to be in balance after the elimination of exterior electric field. The scattering time takes near relative through the electronegativity of an element.

1.3 Power factor

Through study of power factor (PF), the success of a cooler of thermoelectric cooler (TEC) besides generator (TEG) is resolute through study of power factor; it is represented via "PF," and calculated through Seebeck coefficient square multiplied through the electrical conductivity at precise temperature.

Mathematically it can be written as,

$$PF = S^2\sigma \tag{16}$$

In the above equation, PF is Power Factor, S is Seebeck coefficient while σ is Electrical conductivity.

Thermoelectric devices having values of Seebeck coefficient (S) and electrical conductivities high, gives high power factor (PF) and too charitable high electrical power.

1.4 Objectives

Briefly, the specific objectives are as follows:

1. Fabrication of chalcogenides based materials via cost effective chemical synthesis to obtain nanomaterials. Specifically:

    a. Nanostructured n-type Tl_5Te3 via solution co-precipitation and thermos-chemical treatment.

    b. Nanostructured p-type Tl5Te3 via solution co-precipitation and fast chemical reduction.

2. Optimization of critical SPS parameters (such as sintering temperature, applied pressure, holding time and heating rates) for chalcogenides while consolidating these materials to preserve the nanostructure, to reduce thermal conductivity.

3. Bottom-up chemical synthesis and detailed characterization for low temperature TE applications.

4. Fabrication of silicide based TE materials through mechanical alloying (top-down approach). Specifically: a. n-type Tl5Te3 by ball milling for an optimized reaction time and followed by materials' characterizations to identify the phase of the materials.

    a. Doping of Sb and Pb in n-type Tl5Te3 nanomaterials and to investigate its effect on TE performance.

    b. Fabrication of p-type HMS via ball milling by utilizing optimized react followed by detailed physiochemical characterizations.

    c. Study the effect of ternary and quaternary tellurium telluride chalcogenide nanoparticles as nanoinclusions/grain boundary.

5. Optimization of SPS critical parameters (such as sintering temperature, applied pressure, holding time and heating rates) while consolidating these materials to preserve the nanostructure and obtain the desired phases.

1.5 Electrical conductivity and Seebeck coefficient measurements

Figure 2 shows the measurement system that was used to measure the electrical properties of the samples. **Figure 2(a)** displays the photograph of the commercial ZEM-3 system and **Figure 2(b)** shows a sample mounted in the ZEM-3 apparatus for electrical resistivity and Seebeck coefficient measurement. In the ZEM-3 system, electrical resistivity was measured using a four probe technique and electrical conductivity was calculated from the electrical resistivity. The four probe technique for measuring the resistivity simply accounts for the contact resistance between metal electrodes and the semiconducting samples. **Figure 3(a)** displays a schematic diagram of the four probe used by the ZEM-3 system. As shown in **Figure 3(a)**, in the four probe technique current I was passed through one set of probes (blue blocks) and the voltage difference (ΔV) was measured using another set of probes (small red spheres). These four probes were connected to four thermocouples. The voltage and

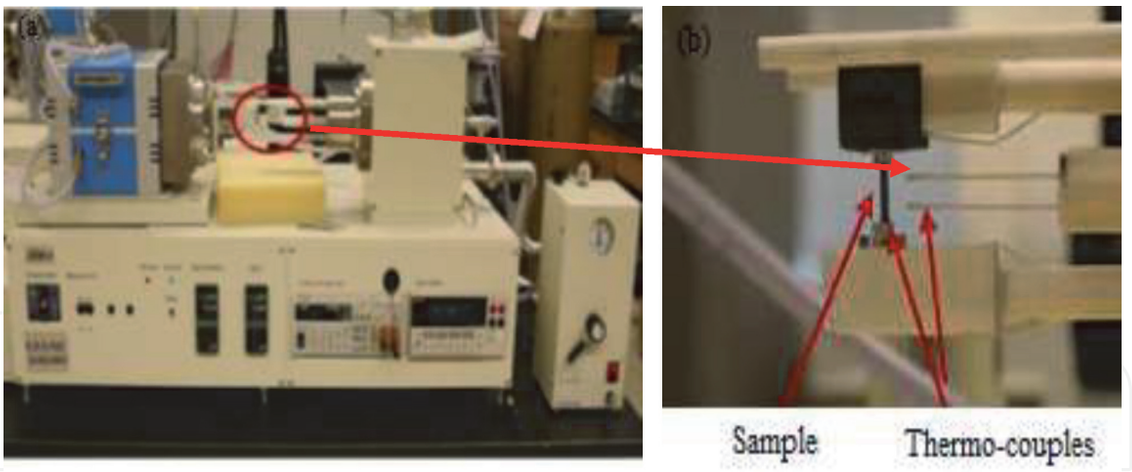

Figure 2.
(a) A commercial ZEM-3 system and (b) magnified sample holder region [indicated by red circle in (a)] with a sample mounted for measurement.

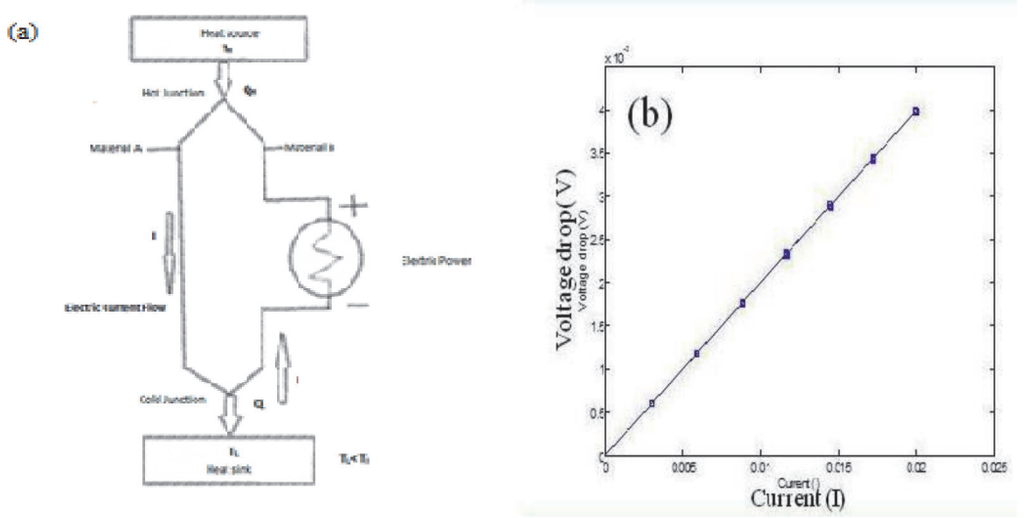

Figure 3.
(a) Displays a schematic diagram of the four probe used by the ZEM-3 system and (b) a typical I-V curve for resistance measurement.

current control, data acquisition, and interpretation were fully automated and computer controlled. The electrical resistivity was found from the relation,

$$\rho = \frac{A}{l}\left(\frac{\Delta v}{\Delta I}\right) \tag{17}$$

Where $(\Delta V/\Delta I)$ is the slope of the I-V curve as shown in **Figure 3(b)**, A is the cross-sectional area of the sample and l is the distance between the voltage probes.

The electrical conductivity was then calculated as the reciprocal of the resistivity.

$$\sigma \alpha \frac{1}{\rho} \tag{18}$$

During the resistivity measurement, the temperatures at both probes were kept constant to minimize the Seebeck voltage. The same ZEM-3 system (**Figure 2**) was used for Seebeck coefficient measurement.

The Seebeck coefficient is simply defined as the ratio of an open-circuit potential difference (ΔV) to a temperature gradient (ΔT),

$$S = \frac{\Delta V}{\Delta T} \tag{19}$$

For Seebeck coefficient measurement, the voltage and temperatures were measured simultaneously by the same thermocouple probe (small red spheres) as shown in **Figure 3(a)**. Then, the voltage difference (ΔV) was measured for a set of temperature differences (ΔT) between the two probes and the Seebeck coefficient was calculated from the slope of ΔV- ΔT plot.

Thallium antimony telluride $TlSbTe_2$ nanoparticles have been prepared by co-precipitation techniques. We have investigated that the electrical resistivity is high and the thermal conductivity is low as compared to Sintered Bi_2Te_3 and TAGS "$(GeTe_{1-x}(AgSbTe_2)_x$" material. The Seebeck coefficient of $TlSbTe_2$ is 224 μvk^{-1} at 666 k which is positive in the whole temperature range showing p-type behavior. The power factor ($S^2\sigma$) found for $TlSbTe_2$ is 8.9×10^{-4} $Wm^{-1}k^{-2}$ at 576 K which is low as compared the power factor of current thermoelectric devices, that is, in the range 10^{-3} $Wm^{-1}k^{-2}$. The figure of merit (ZT) of the order of 0.87 was found at 715 k for $TlSbTe_2$ [1].

Prepared a new low-valent thallium silicon telluride $Tl_6Si_2Te_6$ and compared there results crystal and electronic structure and there electronic properties with $Tl_6Ge_2Te_6$, they observed the same crystal structure of $Tl_6Si_2Te_6$ with $Tl_6Ge_2Te_6$, the quantitative results for $Tl_6Si_2Te_6$. The demerit $[\boldsymbol{Si_6Te_6}]^{2-}$ units crystal structure was found with a single Si-Si bond, the weak bond exist among Tl-Tl and irregularly coordinated by 5 or 6 Te atoms, the black color was observed for both compounds exhibiting a small band gap of the order **0.9 ev** for $Tl_6Si_2Te_6$ and **0.5 ev** for $Tl_6Ge_2Te_6$ compounds. The electrical conductivity and Seebeck coefficient investigated for $Tl_6Si_2Te_6$ is $\mathbf{5.5\ \Omega^{-1}cm^{-1}}$ and $+\mathbf{65\ \mu vK^{-1}}(\boldsymbol{at\ 300\ K})$, while for $Tl_6Gd_2Te_6$ is $\mathbf{3\ \Omega^{-1}cm^{-1}}$ and $+\mathbf{150\ \mu vK^{-1}}(\boldsymbol{at\ 300\ K})$ [2].

Prepared the samples of polycrystalline Ag_9TlTe_5, the different nominal composition by them are: $Ag_9TlTe_x(X\ 5.0, 5.05, 5.1, 5.2, 5.3, 5.5, 5.7, 6.0)$, the Ag_9TlTe_x samples were made by heating the Ag_2Te, Tl_2Te, $Tl_2Te_{1.2}$ and Te with a proper quantity in sealed quartz tube, the ball-milling and hot-press techniques were used for construction of required samples. The X-Ray Diffraction (XRD) technique were used for analysis of phase relation, the electrical resistivity is calculated which is decreasing with increasing temperature except for $Ag_9TlTe_{5.0}$, the investigated Seebeck coefficient is almost independent of temperature except for $Ag_9TlTe_{5.0}$, the power factor is quite high of the order of $0.3 \sim 0.4 \times 10^{-3}$ $Wm^{-1}K^{-2}$ while the power factor for $Ag_9TlTe_{5.0}$ is quite low of the order of0.05×10^{-3} $Wm^{-1}K^{-2}$. The dimensionless thermoelectric figure of merit investigated for $Ag_9TlTe_{5.0}$ is very low approximately 0.08 while for $X \geq 5.0$ is high approximately 1.0, which shows that all the physical properties are changing by changing tellurium content in Ag_9TlTe_x [3].

Herman et al. [4] uses the concept of electronic density of states to increase the thermoelectric figure of merit in lead telluride PbTe, the Seebeck coefficient was enhanced by deforming the electronic density of states, leads to double the thermoelectric figure of merit and he further explained that in nanostructured material it may give us further good results [4].

Synthesized Tl_4MTe_4 $(M = Zr, Hf)$ and investigated their crystal structure and thermoelectric properties, for investigating their crystal structure, the X-ray diffraction technique were used, they found that the crystal structure of Tl_4MTe_4 is octahedral with a space group $R\bar{3}$, the unit cell dimension for Tl_4ZrTe_4 is

$a = 14.6000(5)\ \AA$ and $c = 14.189(1)\ \AA$, and Tl_4HfTe_4 the unit cell dimension is $a = 14.594(1)\ \AA$ and $c = 14.142(3)\ \AA$. Linear muffin-tin orbital (LMTO) methods were used for the calculation of electronic structure clearing that Tl_4MTe_4 exhibit semiconducting behavior exhibiting an indirect band gap of0.3 ev. They observed that the electrical resistivity and Seebeck coefficient decreased while the thermal conductivity increased temperature, the thermoelectric figure of merit (ZT) for Tl_4ZrTe_4 compound increased from 0.14 to 0.1 between the temperature 370 K and 420 K while decreasing when the temperature increased from 420 K, for Tl_4HfTe_4 the ZT varies from 0.05 to 0.09 between temperature 370 K and 540 K [5].

In the other research, prepared the ternary compound Tl_2ZrTe_3 and compared it with Tl_2SnTe_3 and investigated the different properties such as structural, physical and thermal properties. Tl_2ZrTe_3 compound exhibits a simple cubic structure with a lattice parameter $a = 19.118(1)\ \AA$ $(Z = 36)$. They investigated the electronic properties which clears that the Tl_2ZrTe_3 exhibits semiconducting behavior. The band gap observed for Tl_2ZrTe_3 is 0.7 ev which is higher from the band gap of Tl_2SnTe_3 $(Eg = 0.4$ ev), the electrical conductivity is independent of temperature ranging from room temperature to 450 K, when the temperature rises from 450 K the electrical conductivity falls abruptly, while for Tl_2SnTe_3 compound the electrical conductivity decreases from 22 $\Omega^{-1}cm^{-1}$ to 15 $\Omega^{-1}cm^{-1}$ with increasing temperature from room temperature to 515 K, from 373 K to 450 K the thermal conductivity decreases from 0.39 $Wm^{-1}K^{-1}$ to 0.30 $Wm^{-1}K^{-1}$ for Tl_2ZrTe_3 and for Tl_2SnTe_3 the thermal conductivity decreases from 0.24 $Wm^{-1}K^{-1}$ at 420 K to 0.20 $Wm^{-1}K^{-1}$ at 450 K. For Tl_2ZrTe_3 the calculated Seebeck coefficient is generally same in the range of 373 K to450 K, but decreases with temperature greater than450 K, the peak experiential value of Seebeck coefficient is120 μVK^{-1}. For Tl_2SnTe_3 the Seebeck coefficient increases from 240 μVK^{-1} to 330 μVK^{-1} with increasing temperature from room temperature to 450 K. The calculated power factor for Tl_2ZrTe_3 is almost same changes from 0.35 $\mu Wcm^{-1}K^{-1}$ to 0.41 $\mu Wcm^{-1}K^{-1}$ while for Tl_2SnTe_2 the power factor is increasing with temperature. The ZT value of 0.18 at 450 K was observed for Tl_2ZrTe_3 which is less than ZT value of Tl_2SnTe_3 (ZT = 0.31 at 500 K) [6].

Studied the thermoelectric properties of ternary thallium chalcogenides $TlGdQ_2$ (Q = SE, Te) and Tl_9GdTe_6. They found that $TlGdQ_2$ is isostructural with $TlSbQ_2$ and Tl_9GdTe_6 is isostructural with Tl_9BiTe_6. They found the high Seebeck coefficient and low electrical conductivity of $TlGdQ_2$. The low thermal conductivity of the order of 0.5 $Wm^{-1}K^{-1}$was investigated at room temperature for $TlGdTe_2$. In the studies of Tl_9GdTe_6 they found the low power factor due to the high electrical conductivity of 850 $\Omega^{-1}cm^{-1}$ and low seebeck coefficient of 27 μVK^{-1} at550 K. In the whole study they found the good thermoelectric property for $TlGdTe_2$, the dimensionless figure of merit is 0.5 at 500 K [7].

Prepared the thallium lanthanide telluride $Tl_{10-x}Ln_xTe_6$ with Ln = CE, Pr, Nd, Sm, Gd, Tb, Dy, Ho and Er and $0.25 \leq x \leq 1.32$ by hot press method. He found that the crystal structure of $Tl_{10-x}Ln_xTe_6$ is isostructural to Tl_9BiTe_6 and the volume of unit cell is increases with increasing lanthanide content. They investigated that the electrical and thermal conductivity decreases with increasing the lanthanide content while the Seebeck coefficient is increases. In this series for **$Tl_{8.97}Ce_{1.03}$ Te_6, $Tl_{8.92}Pr_{1.08}Te_6$ and $Tl_{8.99}Sm_{1.01}Te_6$** the electrical and thermal conductivity increases and Seebeck coefficient value decreases due to the discontinuity in the band gap as compared to Tl_9LnTe_6 compounds. The power factor is increases with increasing the lanthanide content "x" in the $Tl_{9-x}Ln_xTe_6$ resulting the increase in the dimensionless thermoelectric figure of merit, the best thermoelectric figure of merit

values are 0.22 at 550 K were achieved for the stoichiometric compound on cold press pellets [8].

Fabricate and improve the thermoelectric properties of alumina nanoparticle-dispersed $Bi_{0.5}Sb_{1.5}Te_3$ matrix composites, the nanoparticles were fabricated by ball milling process and followed by spark plasma sintering process. The p-type bismuth antimony telluride (BST) nanopowder prepared from the mechano-chemical process, were mixed with 1.0, 0.5, and 0.3 vol.% with Al_2O_3 nanoparticles by ball milling process. They studied the surface morphology and investigated the size of the nanoparticles. The electrical resistivity is increasing with temperature from 1.5×10^{-5} Ωm at 293 K to 2.5×10^{-5} Ωm at 473 K, and the seebeck coefficient is increases from $+205\,\mu VK^{-1}$ to $+210\,\mu VK^{-1}$ from temperature 293 K to 473 K, respectively, shows p-type semiconducting behavior. The highest Seebeck coefficient of the order of 235 μVK^{-1} at 373 K was observed from 0.3vol.% Al_2O_3/BST nanocomposite. They show that the increasing volume fraction of Al_2O_3 increases the carrier density which affects the Seebeck coefficient, carrier mobility and electrical resistivity of Al_2O_3/BST nanocomposites. The observed power factor is 1.7 times higher from pure BST, that is, 33 μWK^{-2}cm at 393 K for 0.3vol.% Al_2O_3/BST nanocomposites, and for pure BST is22 μWK^{-2}cm. The thermal conductivity is decreased by the addition of Al_2O_3 nanoparticles, for pure BST is 0.8 $Wm^{-1}K^{-1}$ and for Al_2O_3/BST is0.7 $Wm^{-1}K^{-1}$. The thermoelectric figure of merit (ZT) is 1.5 for 0.3vol.% Al_2O_3/BST composite at 373 K which is higher from pure BST [9].

Studied the thermoelectric properties of Indium doped SnTe ($In_xSn_{x-1}Te$) nanostructured compound. They prepared $In_xSn_{x-1}Te$ by ball milling and hot press techniques, and investigated their thermal conductivity, diffusivity and electrical conductivity decreases with temperature ranging from 300 to 900 K, while the power factor and Seebeck coefficient is increases and the specific heat is almost constant a little increase was seen in $In_xSn_{x-1}Te$. The sample is also prepared by ball mill and hand mill method but the result is the same. They observed the relationship of carrier concentration vs. Seebeck effect which shows that In doped SnTe shows abnormal behavior with increasing carrier concentration, they get the SEM, TEM, and HRTEM images of $In_xSn_{x-1}Te$ which clearly shows the sample is consist of both small and large grain boundaries with a good crystallinity which effects the thermal conductivity of the sample. The thermal electric figure of merit is observed which greater than 1 is at temperature 873 K in for $In_{0.0025}Sn_{0.9975}Te$ [10].

Investigated the thermoelectric properties of indium doped $PbTe_{1-y}Se_y$ alloys, solid state method was used for the synthesis. They showed that the carrier concentration and electrical resistivity increases with increasing temperature in n-type indium doped $PbTe_{1-y}Se_y$ alloys affecting the Seebeck coefficient and as a result the power factor of $PbTe_{1-y}Se_y$ alloys. The bipolar effect was observed at high temperature which restricts the thermoelectric figure of merit to 0.66 at 800 K with 30% content in sample; they further concluded that for the enhancement of thermoelectric properties, the increased carrier concentration must be reduced at high temperature [11].

Optimized the thermoelectric properties of $Tl_{10-x-y}Sn_xBi_yTe_6$, a quaternary telluride series has been studied. The crystal structure was investigated by X-Ray diffraction which belongs to Tl_5Te_3 type structure and the volume is increases with increasing the Sn concentration in $Tl_{10-x-y}Sn_xBi_yTe_6$, the electronic structure calculation revealed that $Tl_{8.5}SnBi_{0.5}Te_6$ is a narrow band gap p-type intrinsic semiconductor and $Tl_9Sn_{0.5}$ $Bi_{0.5}Te_6$ is a p-type and narrow band gap extrinsic semiconductor. The electrical conductivity is decreasing with increasing temperature for $Tl_9Sn_{1-y}Bi_yTe_6$, $Tl_{8.67}Sn_{1-y}$ Bi_yTe_6 and $Tl_{8.33}Sn_{1.12}Bi_{55}Te_6$. The low increase of the order of 0.4 $Wm^{-1}K^{-1}$ to 1.4 $Wm^{-1}K^{-1}$was observed in the thermal conductivity of

$Tl_{10-x-y}Sn_xBi_yTe_6$ type materials due to thermal conductivity of electron κ_{el}, and for $Tl_9Sn_{0.2}Bi_{0.8}Te_6$ the thermal conductivity decreases with increasing temperature due to the increase in lattice vibration. The thermoelectric figure of merit, Seebeck coefficient and power factor was increased with increasing temperature, The high power factor $S^2\sigma = 8.1\ \mu Wcm^{-1}K^{-2}$ was observed for Tl_9(Sn, Bi)Te_6 type system, they identified that with low Sn concentration the Seebeck coefficient and power factor is high and at low temperature the power factor is decreases. Yi et al. were study that bulk crystalline ingots into nanopowders by ball milling and hot pressing, in nanostructured bulk bismuth antimony telluride had achieved high figure of merit. He obtained a high value of ZT$\sim$ 1.3 in the temperature range of 75 and 100°*C*. The improvement of ZT is mostly due by the lower of thermal conductivity. TEM observation of microstructure show that the lower thermal conductivity due to the increased of phonon scattering, and increasing of phonon scattering due to the increasing of grain boundaries of nanograins, nanodots, precipitates and defects. When ingot was used as the starting material, the highest ZT value of $\sim$ 0.7 was obtained for bismuth antimony telluride [12].

It is very important for the control of carrier concentration, which is good for thermoelectric properties. Another approach like nanostructuring, the dimensionless figure-of-merit is increased by the reduction of lattice thermal conductivity.

2. Experiment

For the preparation of $Tl_{10-x-y}A_xB_yTe_6$ compounds of different types of dopants (x = Pb, Sn, Ca and y = Pb, Sb, Sr, etc.), with different concentration on tellurium telluride has been prepared by solid state reactions in evacuated sealed silica tubes. The purpose of this study were mainly for discovering new type of ternary and quaternary compounds by using Tl^{+1}, Sn^{+3},Pb^{+3} and etc. Te^{-2} elements as the starting materials [13]. Direct synthesis of stoichiometric amount of high purity elements, that is, 99.99% of different compositions have been prepared for a preliminary investigation. Since most of these starting materials for solid state reactions are sensitive to oxygen and moistures, they were weighing stoichiometric reactants and transferring to the silica tubes in the glove box which is filled with Argon. Then, all constituents were sealed in a quartz tube. Before putting these samples in the resistance furnace for the heating, the silica tubes was put in vacuum line to evacuate the argon and then sealed it. This sealed power were heated up to 650 C^o at a rate not exceeding 1 k/mint and kept at that temperature for 24 hours. The sample was cooled down with extremely slow rate to avoid quenching, dislocations, and crystals deformation. The nanoparticles have been prepared by ball-milling techniques.

Structural analysis of all these samples was carried out by x-rays diffraction, using an Intel powder diffractometer with position-sensitive detector and CuKα radiation at room temperature. No additional peaks were detected in any of the sample discussed here. X-ray powder diffraction patterns confirm the single phase composition of the compounds.

The temperature dependence of Seebeck coefficient was measured for all these compounds on a cold pressed pellet in rectangular shape, of approximately $5 \times 1 \times 1$ mm^3 dimensions. The air sensitivity of these samples was checked (for one sample) by measuring the thermoelectric power and confirmed that these samples are not sensitive to air. This sample exposes to air more than a week, but no appreciable changes observed in the Seebeck values. The pellet for these measurements was annealed at 400 C^0 for 6 hours. For the electrical transport measurements (electrical conductivity) four-probe resistivity technique was used and the pellets were cut into rectangular shape with approximate dimension of $5 \times 1 \times 1$ mm^3.

3. Results and discussions

3.1 Ternary system

3.1.1 Structural analysis

Various concentrations of *Sn* doped $Tl_{10-x}Sn_xTe_6$ compounds series were synthesized, and their physical properties were studied for x = 1, 1.25, 1.50, 1.75, 2.00. The powder x-rays diffraction pattern which is measured at room temperature for all these compounds is presented in **Figure 4**. It is found that the tetragonal single phase $Tl_8Sn_2Te_6$ is obtained in the present study. The tetragonal lattice parameters observed at room temperature are a = 8.8484 nm, and c = 13.0625 nm in table. The materials are iso-structural with the binary tellurium telluride $Tl_{10}Te_6$, and the crystal structure of $Tl_9Sb_1Te_6$ was determined with the experimental formula, possessing the same space group 14/mcm as Tl_5Te_3 and $Tl_8Sb_2Te_6$, in contrast to $Tl_9Sb_1Te_6$ that adopt the space group 14/m. **Figure 5** shows the SEM and EDX images. The SEM shows the morphology of the ternary compound at 100 nm scale.

3.2 Physical properties

3.2.1 Electrical conductivity measurements

We were interested in the effects of Sn doping in parent composition on the border line of semi-conductor and metallic. The experiment was conducted in a commercial oxford instrument cryostat with temperature control better than 0.5 K. the contacts were standard 4-probe, and were made using high quality silver point, contacts resistance was checked at room temperature and experiments were only carried out if it was satisfactorily low, typical current used were of the rate of 0.1 mA.

The electrical properties of tin doped thallium telluride nanostructural system has been investigated under dependency of temperature varying from room temperature 300 to 650K by four probe resistivity technique. It has been founded that Tl_8Sn_2Te6 has the lowest electrical conductivity of 471.6$\Omega^{-1}cm^{-1}$, and when Sn dopant increases from $x = 1.0$ to $x = 2.0$, an electrical conductivity decreases, for example, $\sigma = 471.68\ \Omega^{-1}cm^{-1}$ at $x = 2.0(20\%)$ and $\sigma = 1629.21\Omega^{-1}cm^{-1}$ at $x = 1.0(10\%)$ as shown in **Figure 6**. The electrical conductivity, σ, for the $Tl_{10-x}Sn_xTe_6$ samples with $x < 2.0$ decreases with increasing temperature, **Figure 6**, which clarifies that this decrease in the electrical conductivity is due to the high charge carrier

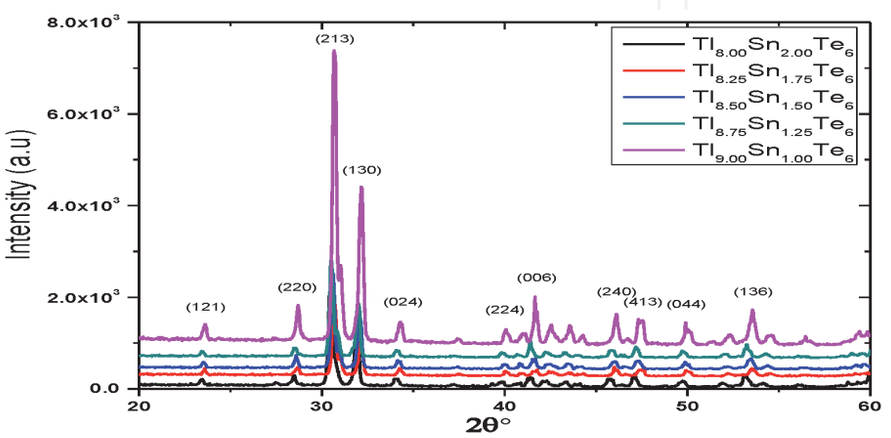

Figure 4.
X-ray diffractometery of $Tl_{10-x}Sn_xTe_6$ doping Sn = 1, 1.25, 1.50, 1.75 and 2.

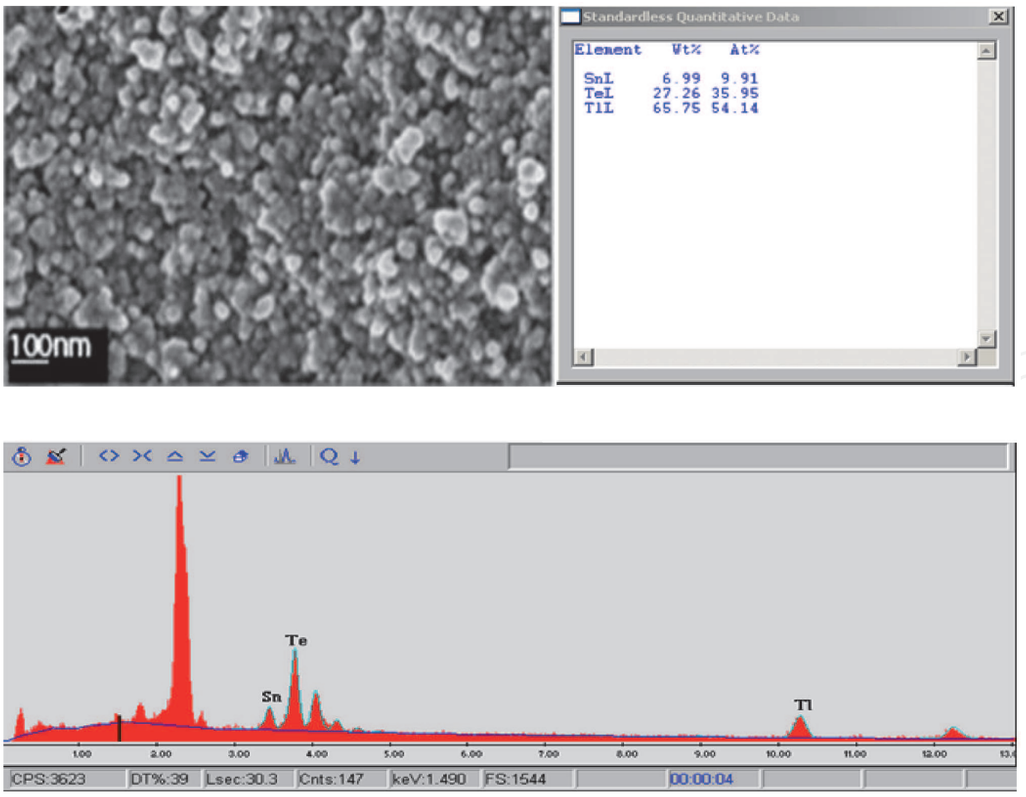

Figure 5.
SEM and EDX image of $Tl_8Sn_2Te_6$.

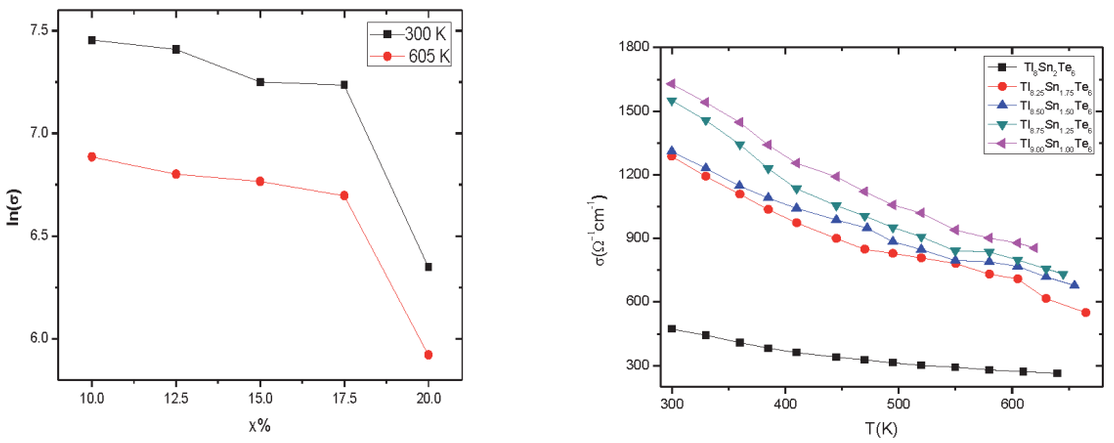

Figure 6.
Electrical conductivity measurements at different concentration and high temperature.

concentration. The highest value has been observed for $Tl_9Sn_1Te_6$ and the lowest value has been observed in sample $Tl_{8.0}Sn_{2.0}Te_6$ at 300*K*. **Figure 6**, shows that the increases the concentration of the dopant decreases the electrical conductivity with temperature of the ternary compounds.

3.2.2 Seebeck coefficient measurements

The positive Seebeck coefficient, S, observed in all samples of $Tl_{10-x}Sn_xTe_6$ as shown in **Table 1**, which increases smoothly with increasing temperature with $1.0 \leq x \leq 2.0$, for p-type semiconductors having high charge carrier concentration (**Table 2**). The Seebeck curve of the sample with x = 2.0 exhibits a clear

Sample	Crystallite size, $D = 0.9\lambda/\beta\cos\theta$ (nm)	Lattice constant a, b, c = (Å)	Volume (Å^3)
$Tl_9Sn_1Te_6$	62.919	a = b = 8.7930 c = 13.0050	1005.505
$Tl_{8.75}Sn_{1.25}Te_6$	63.965	a = b = 8.8450 c = 13.0755	1022.948
$Tl_{8.50}Sn_{1.50}Te_6$	66.2833	a = b = 8.8250 c = 13.0000	1012.44
$Tl_{8.25}Sn_{1.75}Te_6$	59.820	a = b = 8.8100 c = 13.0010	1009.086
$Tl_8Sn_2Te_6$	56.793	a = b = 8.8484 c = 13.0625	1022.717

Table 1.
Crystallite size, lattice constant, and volume of unit cell.

Sample	Electrical conductivity ($\Omega^{-1}cm^{-1}$) at 300K	Electrical conductivity ($\Omega^{-1}cm^{-1}$) at 650K
$Tl_9Sn_1Te_6$	1629.21	939.137
$Tl_{8.75}Sn_{1.25}Te_6$	1550.997	841.481
$Tl_{8.50}Sn_{1.50}Te_6$	1310.326	795.66
$Tl_{8.25}Sn_{1.75}Te_6$	1287.64	781.313
$Tl_8Sn_2Te_6$	471.68	292.102

Table 2.
Electrical conductivity of $Tl_{10-x}Sn_xTe_6(1 \le x \le 2)$ at 300 K and 650 K.

maximum of $S = 79.77 + \mu V.K^{-1}$ at $300K$ and $S = +157.931\mu V.K^{-1}$ at 550 K. The lowest Seebeck coefficient $S = +33.15\ \mu VK^{-1}$ at $300K$ has been observed for $x = 1.0$ which is increases to$S = +65.84\mu V.K^{-1}$ at 550 K, it has been declared that when Sn content increase in host sample the Seebeck coefficient S, also increases, for example, for $x = 1.0$ the Seebeck coefficient has been observed is $S = +33.15\mu VK^{-1}$ to $S = +79.77\mu V.K^{-1}$ for at 300 K and the Seebeck coefficient has been observed is $S = +65.844\ \mu VK^{-1}$ to $S = +157.937\mu V.K^{-1}$ for $x = 2.0$ at 550 K, respectively as shown in **Figure 7**. The power factor of S_n doping is increases as the temperature is increase as shown in **Figure 8**.

3.2.3 Power factor analysis

The power factor investigations show that it increases because of increasing behavior in Seebeck coefficient with temperature (**Table 3**). The calculated power factor is directly proportional to the square of the Seebeck coefficient and the electrical conductivity. The lowest power factor $1.9\mu Wcm^{-2}K^{-2}$ has been observed for $Sn = 1$ and the highest power factor $7.579\mu Wcm^{-2}K^{-2}$ has been observed for $Sn = 1.75$ at temperature $300K$, while for $Sn = 2$ the power factor is $3.639\mu Wcm^{-2}K^{-2}$ as shown in **Table 4**, which is increases with increasing temperature; this low power factor has been observed due to extremely low electrical conductivity of $Tl_8Sn_2Te_6$ which play a man role in the investigation of power factor.

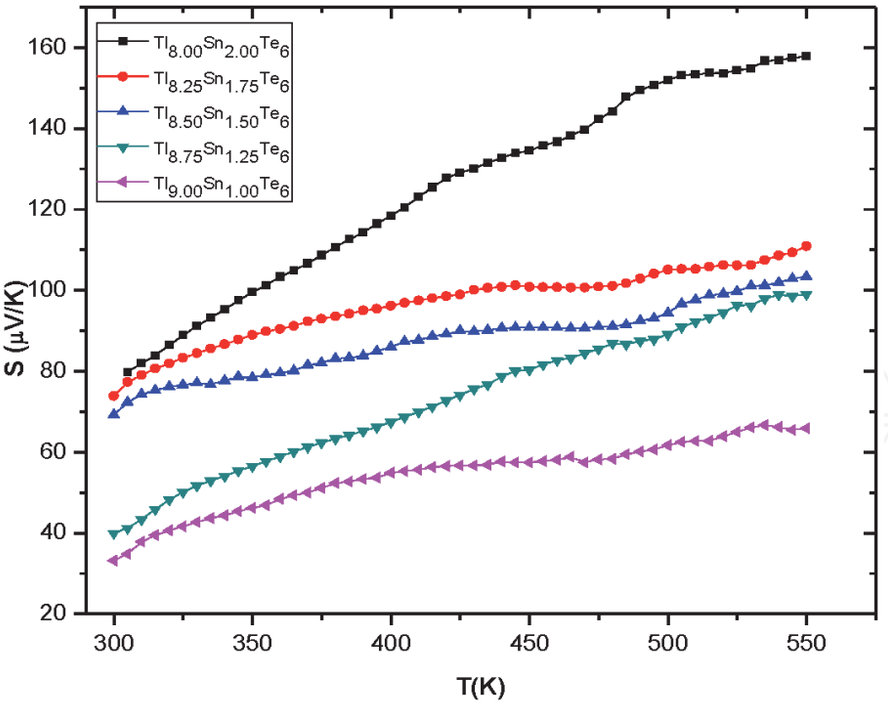

Figure 7.
Seebeck coefficient measurements of $Tl_{10x}Sn_xTe_6$ $(1 \leq x \leq 2)$ at 300K and 550K.

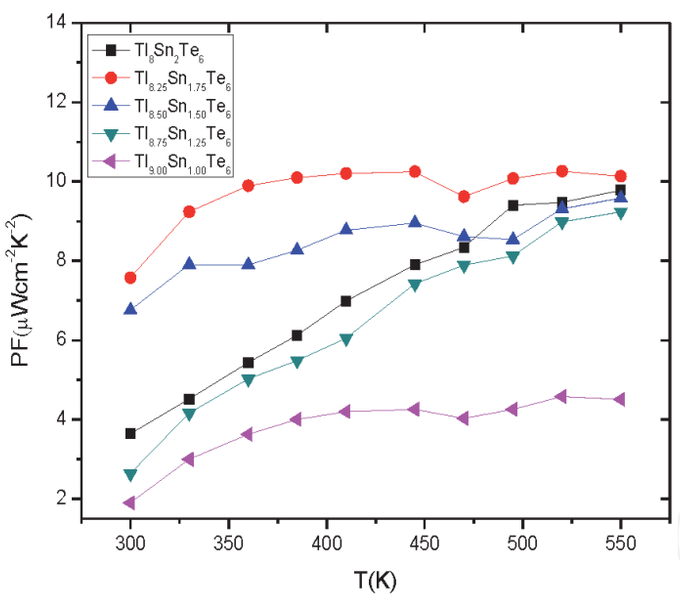

Figure 8.
The power factor (PF) of $Tl_{10-x}Sn_xTe_6$ with $x = 1, 1.25, 1.50, 1.75,$ and 2.

Sample	Seebeck coefficient (μVK^{-1}) at 300K	Seebeck coefficient (μVK^{-1}) at 550K
$Tl_9Sn_1Te_6$	33.15	65.844
$Tl_{8.75}Sn_{1.25}Te_6$	39.953	99.035
$Tl_{8.50}Sn_{1.50}Te_6$	69.207	103.419
$Tl_{8.25}Sn_{1.75}Te_6$	73.879	110.958
$Tl_8Sn_2Te_6$	79.77	157.931

Table 3.
Thermoelectric properties of $Tl_{10-x}Sn_xTe_6(1 \leq x \leq 2)$ at 300 K and 550 K.

3.3 Quaternary System

3.3.1 Structural analysis

X-ray diffraction is the greatest and significant method for the investigation of crystal structure of nanomaterials. With the purpose, to check the purities of different phases of compound peaks in XRD figures, as per revealed in **Figure 9**. It is authenticated that the XRD design of all these samples are fine unchanging with the literature and has been recognized that the crystal structure scheme is isostructural with reference data of Tl_9GdTe_6 and Tl_9BiTe_6 having tetragonal crystal structure with the space group symbol of 4/cm. The SEM shows, morphological structure at the 100 nm scale. The energy dispersion X-ray diffractometer show the concentrate composition of the compound in **Figure 10**.

3.4 Physical properties

3.4.1 Electrical conductivity measurements

The temperature variations of electrical conductivity of quaternary compounds are revealed in **Figure 11**. The conductivity experiential for the entire samples are studied here, decreases with increasing temperature, representing the degenerate semiconductor performance because of positive temperature coefficient, subsequent from the phonons scattering of charge carriers and grains boundaries effects.

Sample	Power factor ($\mu W cm^{-2}K^{-2}$)at 300 K	Power factor ($\mu W cm^{-2}K^{-2}$) at 550 K
$Tl_9Sn_1Te_6$	1.9	4.505
$Tl_{8.75}Sn_{1.25}Te_6$	2.637	9.234
$Tl_{8.50}Sn_{1.50}Te_6$	6.755	9.579
$Tl_{8.25}Sn_{1.75}Te_6$	7.574	10.135
$Tl_8Sn_2Te_6$	3.638	9.777

Table 4.
Power factor of $Tl_{10-x}Sn_xTe_6 (1 \leq x \leq 2)$ *at* 300 K *and* 550 K.

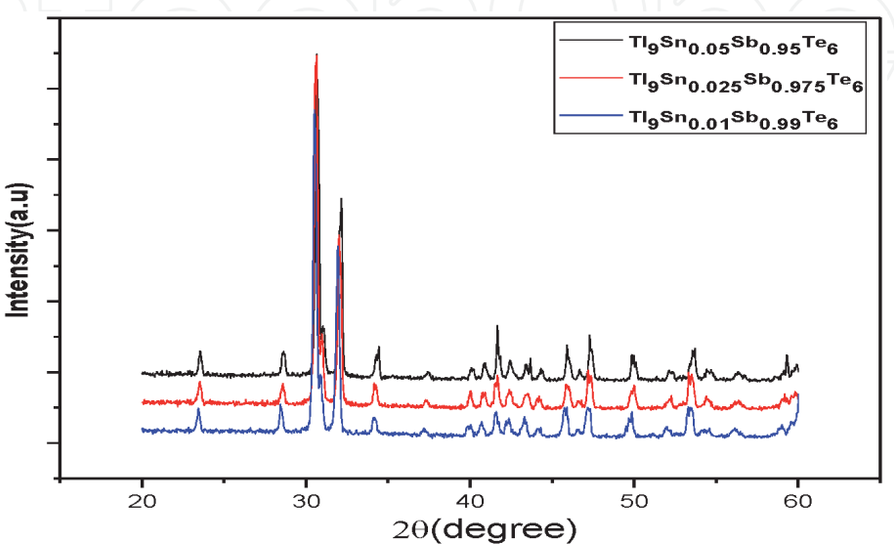

Figure 9.
XRD data of $Tl_9(SnSb)_1Te_6$ *with Sn = 0.01, 0.025 and 0.05.*

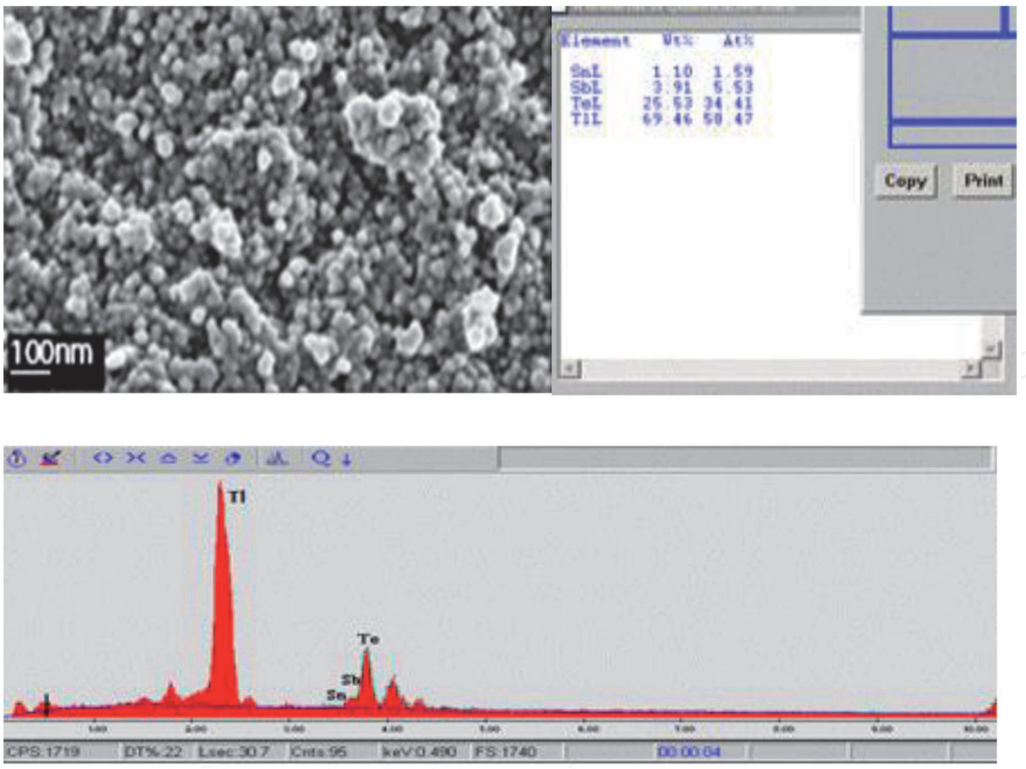

Figure 10.
SEM and EDX image of $Tl_9(SnSb)_1Te_6$.

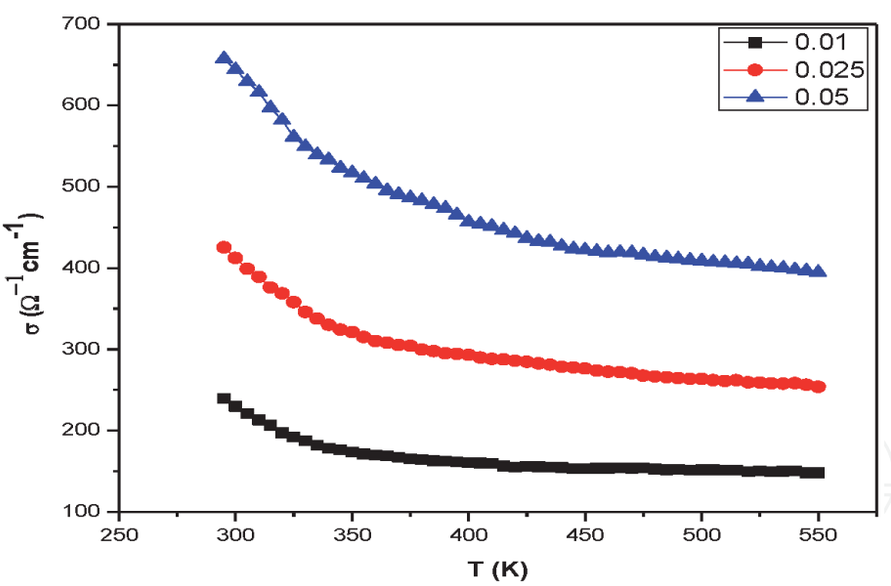

Figure 11.
Electrical conductivity measurements at different high temperature.

An increasing "*x*" value (i.e. increasing the Sn deficiency) is predictable to increase the number of holes, which is experimental detected. The smaller temperature need may be produced by (less temperature dependence) more grain boundary scattering. No systematic trend was found in the variation of the electrical resistivity for samples $Tl_9Sb_{1-x}Sn_xTe_6$ (x = 0.01, 0.025, and 0.05) with "Sn" concentration. The low electrical conductivity in the pressure less sintered sample may be caused by means of the oxide impurity phase in the grain boundary and the number of the grain boundary. The *Sn* doping level and grain boundary resistance may play significant part for increasing electrical conductivity.

3.4.2 Seebeck coefficient (S) analyses

To examine the influence of decrease of the charge carriers in thermal and transport features, Sn content was increased in $Tl_9Sb_{1-x}Sn_xTe_6$ (x = 0.01, 0.025, and 0.05) by means of replacing Sb atoms conferring to the formula. The temperature variation as a function of the Seebeck coefficient (S) for the $Tl_9Sb_{1-x}Sn_xTe_6$ (x = 0.01, 0.025 and 0.05) compounds are revealed in **Figure 12**. The Seebeck coefficient was measured in the temperature gradient of 1 K. The positive Seebeck coefficient increases easily with increasing temperature from 300 K to 550 K, for all compounds in mainly for p-type semiconductors having high charge carrier concentration. It is understandable that all the samples display positive Seebeck coefficient for the whole temperature range, signifying that the p-type (hole) carrier's conduction controls the thermoelectric transportation in these compounds. When the amount of Sn increased from 0.01 to 0.05, the Sn doping is supposed to increase the carrier's density. Though, the smaller grains upon Sn doping are thought to be talented to improve the electron scattering, yielding an increase of the Seebeck coefficient and effective mass.

3.4.3 Power factor calculation and analysis

To improve the power factor (PF = $S^2\sigma$) for these compounds, we require to decouple the electrical conductivity from the Seebeck coefficient, typically inversely proportional to each other in these systems. The key contribution in the "PF" originates from the Seebeck coefficient, so we must design the materials such that their "S" should be improved. The power factors calculated from the electrical conductivity "σ" and the square of Seebeck coefficient "S," gotten for $Tl_9Sb_{1-x}Sn_xTe_6$ compounds with x = 0.01, 0.025 and 0.05 are showed in **Figure 13**. The power factor increases with increasing temperature for all these compounds. The doping concentration demonstrations a systematic effect on the power factor as increasing the doping concentration, the power factor is increases. The

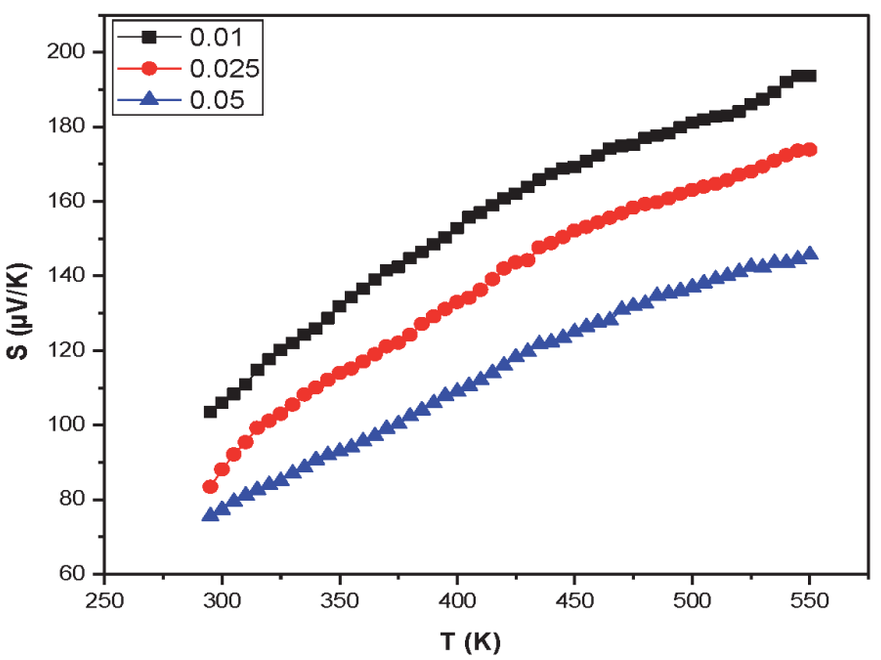

Figure 12.
Seebeck coefficient measurements at different concentration and high temperature (0.01, 0.025, 0.05).

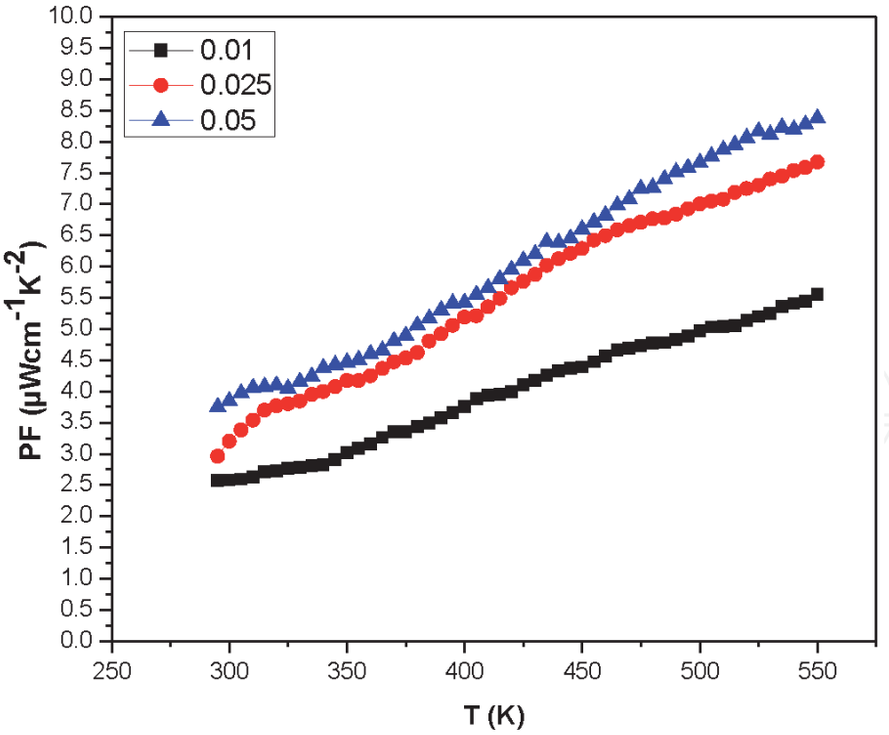

Figure 13.
*The power factor (*PF*) of $Tl_9Sb_{1-x}Sn_xTe_6$ with $x = 0.01, 0.025, 0.05$.*

$Tl_9Sb_{0.95}Sn_{0.05}Te_6$ compound showed the highest value 8.37 (μWtt-cm^{-1}-K^{-2}) of "PF" at 550 K and 3.75 (μWtt-cm^{-1}-K^{-2}) at 295 K. The lowest "PF" were experiential for $Tl_9Sb_{0.99}Sn_{0.01}Te_6$ compound which have values of 5.55 (μWtt-cm^{-1}-K^{-2}) at 550 K and 2.56 (μWtt-cm^{-1}-K^{-2}) at 295 K. As deliberated earlier, an increasing the "Sn" contents are probable to increase the number of holes and the dominant charge carriers.

4. Conclusion

In this study, the ternary and quaternary Tellurium Telluride chalcogenides, $Tl_{10-x-y}A_xB_yTe_6$ nanoparticles, with different types of dopants (A = Sb, and B = Sn) and with different concentration of Sn has been introduced to synthesize new materials by co-precipitation techniques and explored their structural, electrical and thermal properties has been analyzed in details. The structural investigation revealed that $Tl_{10-x}Sn_xTe_6$ is isostructural with Tl_5Te_3 with a same space group I4/mcm. All peaks are corresponding to their respective element, and no extra peaks are observed, which shows that we got a correct crystal structure for our design materials and also shows that no impurities or dislocation in the sample has been observed. An energy dispersive X-ray spectroscopy was used for the confirmation of elemental and compositional ratio of all the samples studied here. The electrical characterizations shows that parent compounds behaves like a semiconductor, but increasing the Sn contents, this materials tend toward the metallic properties, which show that increasing the temperature the electrical conductivity will decreases. The electrical characterizations show that parent compounds behaves like a semiconductor, but increasing the *Sn* contents, this nanomaterials tend to metallic phase, which display that increasing the temperature the electrical conductivity will decreases at higher temperature.

All samples exhibited positive S values, increasing Sn-filling, the Seebeck coefficient increased due to increase in its metallic behavior and low thermal conductivity. By increasing the temperature, the Seebeck coefficient was increased and the highest Seebeck coefficient was observed for $Tl_8Sn_2Te_6$; $S = +157\mu VK^{-1}$. Consequently, power factor was enhanced and increased with high Sn concentration up to Sn = 1.75 and the maximum power factor $(PF = 7.579\mu Wcm^{-2}K^{-2})$ was observed for $Tl_{8.25}Sn_{1.75}Te_6$. The reduction in the power factor for $Tl_8Sn_2Te_6$ is due to their low electrical conductivity. The thermopower is positive in the whole temperature range studied here, which is increasing with increase in temperature, representing that the nanoparticles under study is hole conduction dominated. For higher concentrations of *Sn*, the Seebeck coefficient of the doped tellurium telluride is decreasing because of increasing the holes concentration which in turns increasing the electron scattering in this doped chalcogenide system. However, the smaller grains upon Sn concentrations will improve the electron scattering, resulting increase in thermos-power. Therefore, power factor was improved and increased with high "Sn" concentration up to Sn = 0.05 and the maximum power factor (PF = 8.37 $\mu Wcm^{-1}K^{-2}$) was observed for $Tl_9Sb_{0.95}Sn_{0.05}Te_6$. This enhanced power factor will improve the thermoelectric efficiency and results decent thermoelectric applications, which is the key goal of this study. At the end, we are going to accomplish that this work is the finest example of enhancing dopants concentration to attain required thermoelectric properties in "*Sn*" doped $Tl_9Sb_{1-x}Sn_xTe_6$ chalcogenide system. To understand our results, we start by final the basic understanding of the metallic long-range interactions due to do the injections of charge carriers concentration, and semiconducting frustration effects fore-most to metallic like conduct in these chalcogenides.

Author details

Wiqar Hussain Shah* and Waqas Muhammad Khan
Department of Physics, Faculty of Basic and Applied Sciences, International Islamic University, Islamabad, Pakistan

*Address all correspondence to: wiqar.hussain@iiu.edu.pk

References

[1] Kurosaki K, Uneda H, Muta H, Yamanaka S. Thermoelectric properties of thallium antimony telluride. Journal of Alloys and Compounds. 2004:43-48

[2] Assoud A, Soheilnia N, Kleinke H. Crystal structure, electronic structure and physical properties of the new low-valent thallium silicon telluride Tl6Si2Te6 in comparison to Tl6Ge2Te6. Journal of Solid State Chemistry. 2006; **179**:2707-2713

[3] Kurosaki K, Goto K, Muta H, Yamanaka S. Fabrication and thermoelectric properties of Ag9TlTeX (X=5:0∼6:0). Materials Transactions. 2007;**48**(8):2083-2087

[4] Heremans JP, Jovovic V, Toberer ES, Saramat A, Kurosaki K, Charoenphakdee A, et al. Enhancement of thermoelectric efficiency in PbTe by distortion of the electronic density of states. Science. 2008;**321**:554-557

[5] Sankar CR, Sanasy SB, Assoud A, Kleinke H. Syntheses, crystal structures and thermoelectric properties of two new thallium tellurides: Tl4ZrTe4 and Tl4HfTe4. Journal of Materials Chemistry. 2010;**20**:7485-7490

[6] Sankar CR, Guch M, Assoud A, Kleinke H. Structural, thermal, and physical properties of the thallium zirconium telluride Tl2ZrTe3. Chemistry of Materials. 2011;**23**: 3886-3891

[7] Raj C, Savitree BS, Holger K. Thermoelectric properties of TlGdQ2(Q = Se, Te) and Tl9GdTe6. Journal of Electronic Materials. 2012;**41**(6): 1662-1666

[8] Sanasy SB. Thermoelectric properties of Tl10-xLnxTe6, with Ln=Ce, Pr, Nd, Sm, Gd, Tb, Dy, and Er, and 0.25<x< 1.32. Journal of Alloys and Compounds. 2013:126-134

[9] Kim KT, Ha GH. Fabrication and enhanced thermoelectric properties of alumina nanoparticle-dispersed Bi0.5Sb1.5Te3 matrix composites. Journal of Nanomaterials. 2013;**2013**:1-6

[10] Zhang Q, Liao B, Lan Y, Lukas K, Liu W, Esfarjani K, et al. High thermoelectric performance by resonant dopant indium in nanostructured SnTe. Applied Physical Sciences. 2013;**110**(33): 13261-13266

[11] Bali A, Wang H, Snyder GJ, Mallik RC. Thermoelectric properties of indium doped PbTe1-ySey alloys. Journal of Applied Physics. 2014;**116**: 033707

[12] Kuropatwa BA, Guo Q, Assoud A, Kleinke H. Optimization of the telluride Tl10–x–ySnxBiyTe6 for the thermoelectric energy conversion. Journal of Inorganic and General Chemistry. 2014;**640**:774-780

[13] Dresselhaus MS, Chen G, Tang MY, Yang RG, Lee H, Wang DZ, et al. New directions for low-dimensional thermoelectric materials. Advanced Materials. 2007;**19**(8):1043-1053